

Article

Study on Dynamic Mechanical Behaviors and J–C Constitutive Model of a Fine-Grained D6A Steel

Zezhou Yang ¹, Xiaowei Feng ^{1,*}, Xiaoli Zhang ², Yongfeng Shen ² , Xicheng Huang ¹ and Ruoze Xie ¹ 

¹ Institute of Systems Engineering, China Academy of Engineering Physics, Mianyang 621999, China; yangzzxx@foxmail.com (Z.Y.); huangxc@caep.cn (X.H.); xierz@caep.cn (R.X.)

² Key Laboratory for Anisotropy and Texture of Materials, Northeastern University, Shenyang 110819, China; zhxiaoli001@163.com (X.Z.); shenyf@smm.neu.edu.cn (Y.S.)

* Correspondence: 414fengxw@caep.cn; Tel.: +86-0816-2485474

Abstract: The uniaxial tensile loading tests of coarse-grained D6A steel (CG, $d = 20 \mu\text{m}$) and fine-grained D6A steel (FG, $d = 1.5 \mu\text{m}$) were performed using a material testing machine and rotating disk Hopkinson tension bar, respectively. The stress–strain curves of two steels at different strain rates ($0.001\text{--}1500 \text{ s}^{-1}$) were obtained. Results show that grain refinement effectively improves the strength of FG steel, which is achieved by high-density of grain boundaries and cementite particles hindering the movement of dislocations. In the strain rate range of the test, the strain rate sensitivity of FG D6A steel decreases, which is considered to be the result of the athermal stress that independent of the strain rate becomes the dominant part of the total stress. Combined with the experimental data, the parameters of the Johnson–Cook (J–C) constitutive model were calibrated. The stress–strain curves obtained by simulations are in good agreement with those from tests. These results may provide an important experimental reference and theoretical basis for the application of FG D6A steel in various fields.

Keywords: fine-grained D6A steel; fine grain strengthening; strain rate sensitivity; Johnson–Cook constitutive model; finite element simulation



Citation: Yang, Z.; Feng, X.; Zhang, X.; Shen, Y.; Huang, X.; Xie, R. Study on Dynamic Mechanical Behaviors and J–C Constitutive Model of a Fine-Grained D6A Steel. *Crystals* **2022**, *12*, 806. <https://doi.org/10.3390/cryst12060806>

Academic Editors: Yong He, Wenhui Tang, Shuhai Zhang, Yuanfeng Zheng and Chuanting Wang

Received: 29 April 2022

Accepted: 26 May 2022

Published: 7 June 2022

Publisher's Note: MDPI stays neutral with regard to jurisdictional claims in published maps and institutional affiliations.



Copyright: © 2022 by the authors. Licensee MDPI, Basel, Switzerland. This article is an open access article distributed under the terms and conditions of the Creative Commons Attribution (CC BY) license (<https://creativecommons.org/licenses/by/4.0/>).

1. Introduction

The production, use and performance improvement of steel materials are important to develop industrialization. For thousands of years, steel has been widely used in various engineering fields such as civil engineering, chemical engineering, aerospace and weaponry, and has profoundly affected the quality of human life. In recent years, aerospace materials continue to evolve, new materials represented by graphene, carbon fiber and rare earth elements are favored by researchers, but they still cannot surpass high-property steel in terms of material strength, impact toughness and production cost. In the future, ultra-high-strength steel will still be an indispensable material for load-bearing components such as aircraft landing gear, wing spars, and engine crankshafts. In order to meet the rapid development needs of the aviation industry, it is necessary to deeply explore the strengthening mechanism and application prospects of advanced steel materials.

Due to the lightweight and safety requirements of aircraft design, materials with high strength and toughness will be the first choice for airframe components. Ultra-fine-grained (UFG) steel has both ultra-high strength, good toughness [1] and low production cost, which has great application potential in the aviation industry. At present, scholars in China and abroad have carried out extensive research on the preparation process and mechanical properties of UFG steel. Pang [2] investigated the strengthening mechanism of low-temperature annealed UFG steel, and believed that grain refinement was the most effective method to simultaneously improve the strength, plasticity and impact toughness of the material. The strengthening of the experimental steel was not only the result of the interaction between dislocations, but also the interaction of grain boundaries and

dislocations. Park [3] found that when the grains are refined to less than a few microns, the strength can be effectively improved. However, the material almost loses the work hardening ability, and its yield ratio is close to 1. Liu et al. [4] studied the effects of strain rate and temperature on the dynamic mechanical behavior of UFG IF steel. They found that UFG IF steel has low strain rate sensitivity and strong temperature sensitivity within a certain temperature range ($-70\text{ }^{\circ}\text{C}$ – $100\text{ }^{\circ}\text{C}$). To sum up, the mechanical behavior of UFG steel is closely related to the microstructure (e.g., grain size) and loading conditions (e.g., strain rate, temperature).

Aircraft often face high-speed impact during landing, so it is of great significance to study the dynamic mechanical properties of structural component materials. At present, establishing a macroscopic phenomenological constitutive model or modifying the existing phenomenological model is the main method to describe the mechanical behavior of UFG materials. Khan [5] modified the Johnson–Cook (J–C) to describe the flow stress of nanometallic materials by introducing the Hall–Petch relationship between yield stress and grain size. Zheng et al. [6] introduced the grain size effect on the basis of the J–C model, and then superimposed it with the Armstrong–Frederick nonlinear hardening law. Finally, they proposed a mixed hardening model for UFG materials, which can simultaneously reflect the nonlinear hardening, grain size effect, strain hardening effect and strain rate effect of the material. Based on the modified hyperbolic sine Arrhenius equation, Wang [7] established a constitutive model capable of simulating high temperature micro-compression deformation of UFG pure aluminum. Therefore, building a constitutive model capable of describing large plastic deformation is the basic to promote the practical application of advanced steel materials.

D6A steel is a low-alloy high-strength steel that has been widely used in solid rocket casings, aircraft landing gear, warhead casings and other fields. Shen et al. [8–12] prepared micron-scale fine-grained (FG) D6A steel by using hot rolling and annealing, and analyzed the influence of grain size and nano-precipitation relative to the strength and toughness of FG steel. Grain refinement strengthening, precipitation phase strengthening and texture strengthening are the main mechanisms for the high strength of the investigated steels. Currently, several studies have extensively investigated FG D6A steel, and most of them focus on the preparation process and microstructure evolution. However, its mechanical behavior at dynamic loading was rarely reported. The present study aims to provide experimental and theoretical reference for the use of FG D6A steel in the aviation field.

2. Experimental Materials and Test Methods

The experiment material is D6A coarse-grained (CG) steel, which was produced by Baosteel Group. The D6A steel was forged into a slab with 110 mm in length, 60 mm in width, and 60 mm in thickness. First, in the process of hot rolling, the steel plate was heated to $1100\text{ }^{\circ}\text{C}$ for 3 h, and then hot-rolled to a thickness of 10 mm after six passes. Then, the plate underwent two-phase warm rolling at $760\text{ }^{\circ}\text{C}$ via two passes with $\sim 25\%$ reduction in each pass, and annealing at $660\text{ }^{\circ}\text{C}$ for 20 min after each pass. After hot rolling and two-phase annealing, FG D6A steel samples were obtained. The nominal chemical composition of the steel, measured by using chemical analysis, is listed in as Table 1. The microstructure of FG D6A steel before deformation was characterized by scanning electron microscope (SEM) after polishing and acid leaching. As shown in Figure 1, the investigated steel is mainly composed of gray-black ferrite matrix (F) and white granular cementite (Fe_3C). During the hot rolling process, a large amount of spherical cementite precipitates from the grain boundary and is evenly distributed on the ferrite matrix.

Table 1. Chemical composition of the D6A steel (mass fraction%).

C	Si	Mn	Cr	Mo	Al	Ni	V	Fe
0.43	0.17	0.73	1.05	1.01	0.02	0.61	0.09	Bal

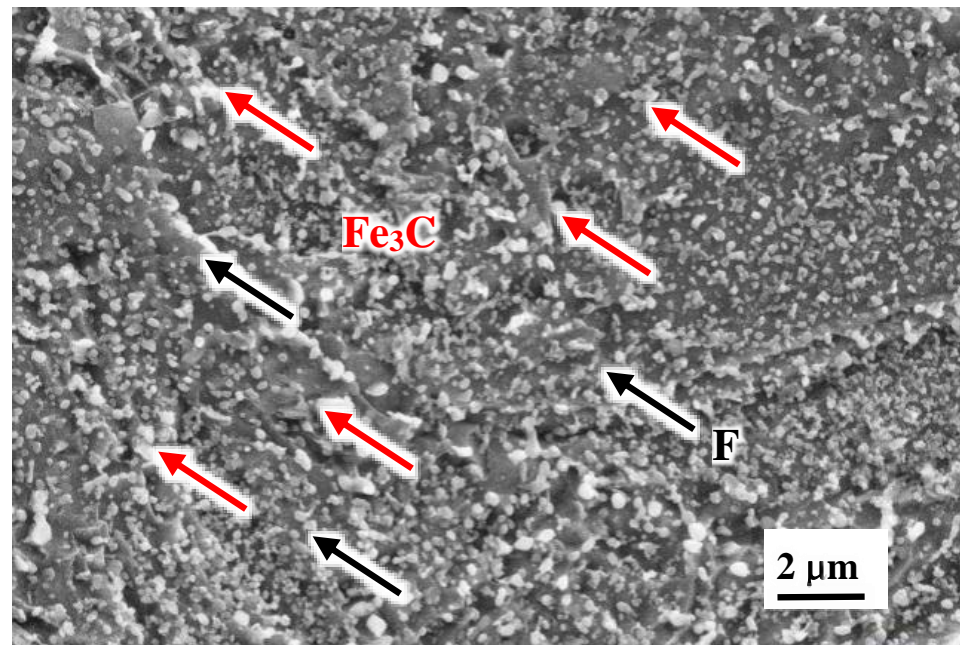


Figure 1. SEM images showing the microstructural characteristics of FG D6A steel.

Figure 2 shows the microstructure of FG steel obtained from electron backscatter diffraction (EBSD) microscopy. At the same time, the EBSD observation data were statistically sorted by Origin software, and the columnar distribution of grain size was obtained, as shown in Figure 3a,b. The grain size of CG and FG D6A steel was 20 μm and 1.5 μm , respectively.

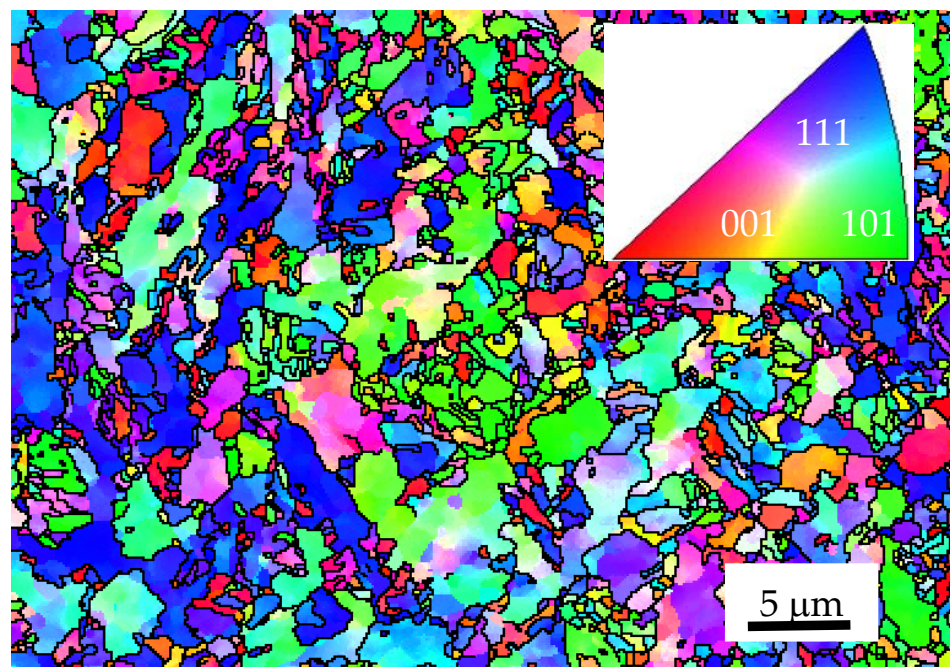


Figure 2. EBSD graph of FG D6A steel.

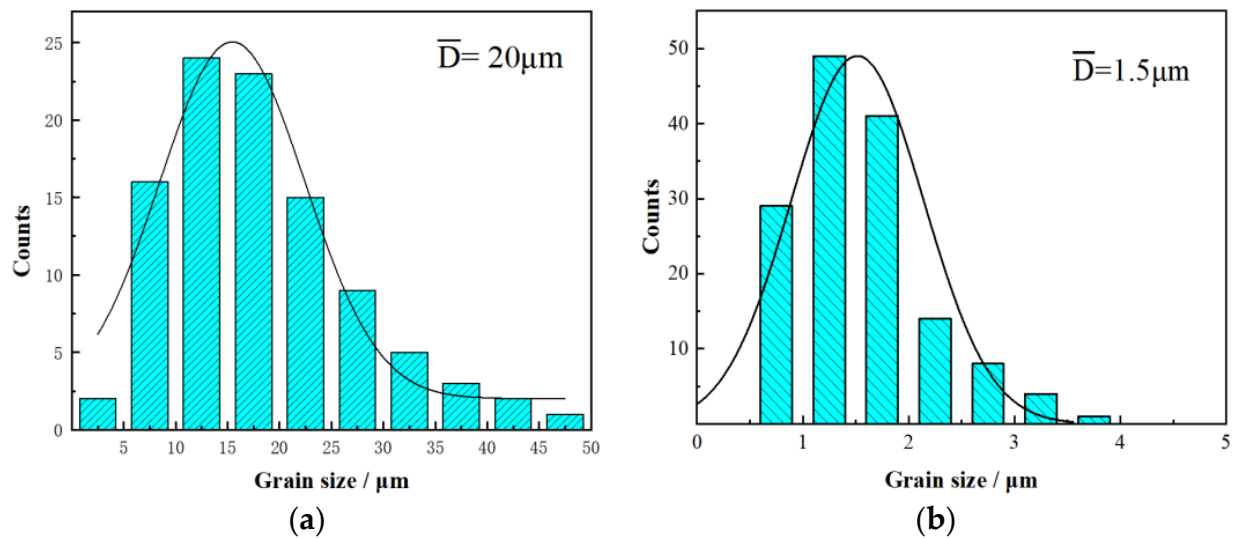


Figure 3. Grain size distributions of D6A steel: (a) CG D6A steel; (b) FG D6A steel.

Uniaxial tensile tests were carried out on the specimens at room temperature. Quasi-static tensile experiment was performed on a material testing machine and dynamic tensile test was carried out on a rotating disk Hopkinson bar. The steel was prepared into a sheet specimen and connected with the loading device by gluing. Figure 4a,b show the experimental device and specimen. Dynamic uniaxial tensile tests were conducted at various strain rates ($\dot{\epsilon}$) ($400\sim 1500\text{ s}^{-1}$) by using short metal rods with different sizes (8, 10 and 12 mm). For comparison, similar tensile experiments were performed on CG steel.



Figure 4. Photographs of Hopkinson tension bar and specimen in this study: (a) rotating disk Hopkinson bar; (b) steel specimens.

3. Experimental Results and Discussion

The experimental data were processed by the signal acquisition system embedded in the equipment and transformed by Origin software to obtain the stress–strain curves of the steel under different strain rates.

Figure 5a shows the representative stress–strain curves of the as-prepared CG steel, which was tested at room temperatures of $25\text{ }^{\circ}\text{C}$ at a strain rate ($\dot{\epsilon}$) of 0.001 s^{-1} , and the experiment was repeatable. The quasi-static tensile yield strength of FG D6A steel is approximately 980 MPa (curve turning point in the figure), which is significantly improved compared with that of existing CG steel (390 MPa [9]).

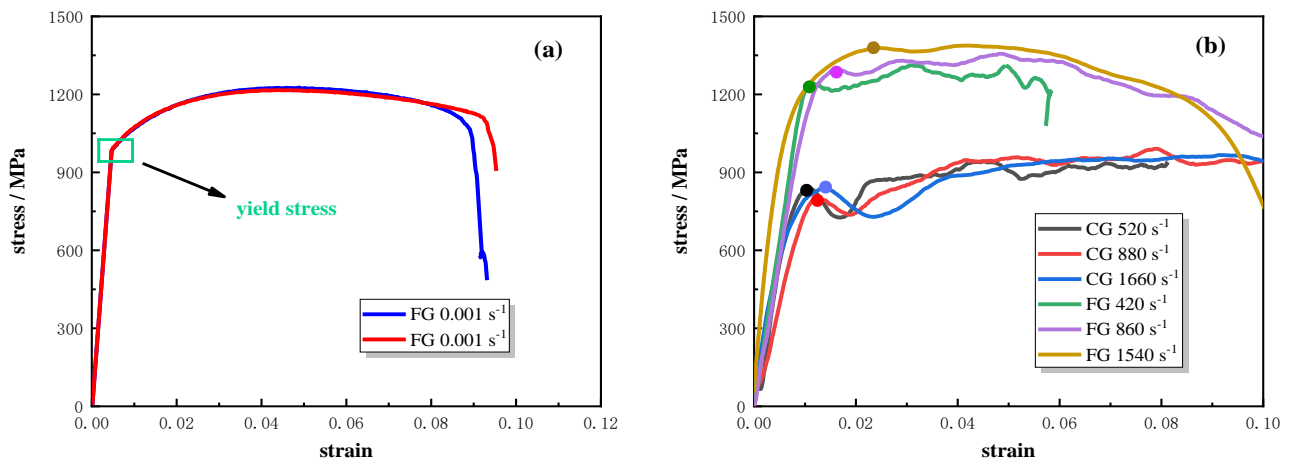


Figure 5. Stress–strain curves of the investigated steel under different strain rates: (a) quasi–static loading; (b) dynamic loading.

The dynamic tensile tests of the CG ($\dot{\epsilon} = 520, 880, 1660 \text{ s}^{-1}$) and FG ($\dot{\epsilon} = 420, 860, 1540 \text{ s}^{-1}$) D6A steel were carried out, and the obtained stress–strain curves are shown in Figure 5b. It is worth noting that the first peak stress can be regarded as material strength under dynamic loading (as indicated by the dots in the figure). In this experiment, the dynamic strength of CG steel is about 800 MPa, whereas that of FG steel is over 1300 MPa. The strength of the investigated steel at various strain rates are shown in Table 2. In summary, grain refinement effectively improves the static and dynamic strength of D6A steel.

Table 2. Tensile mechanical properties of D6A steel at room temperature.

Temperature/ $^{\circ}\text{C}$	Grain Size	Strain Rate/ s^{-1}	Strength/Mpa
25	FG	0.001	980
		420	1245
		860	1295
		1540	1378
		0.017	390
	CG	520	838
		880	800
		1660	835

Similar to CG steel, the grains of FG steel still exhibit typical crystallographic characteristics, and the microstructure profoundly affects the macroscopic mechanical behavior of materials. High-density grain boundaries have a strong constraint on dislocation slip, which is mainly caused by grain boundary obstacles and the orientation difference between adjacent grains. Due to the disordered arrangement of atoms at grain boundaries, the shear stress required for dislocation slip here increases suddenly. Furthermore, grains in different orientations will restrict mutual deformation, which makes it difficult for slip to proceed along the same crystal axis and eventually increases the critical shear stress of slip. Figure 6 shows that when the external force is not large enough to overcome the obstacle effect of grain boundary, the intragranular dislocation cannot continue to slip through the grain boundary to the adjacent crystal. With the accumulation of deformation, dislocations gather at the grain boundary and tangle with each other to produce dislocation pile-up groups, resulting in local stress concentration (shown in the red symbol), thereby improving the macroscopic strength of the investigated steel.

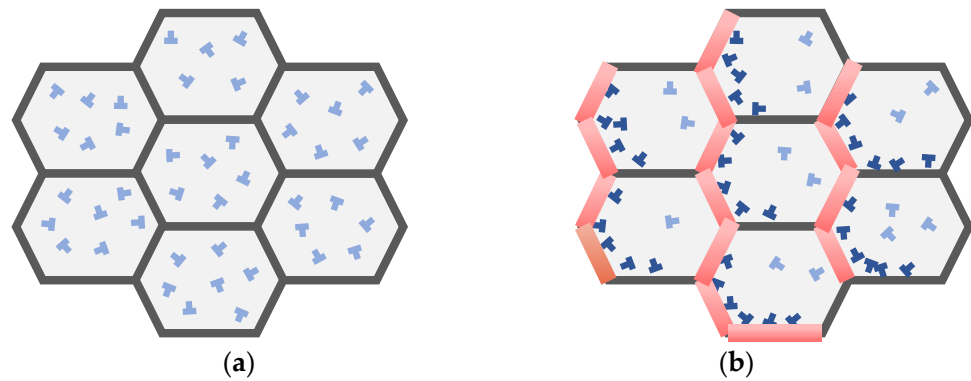


Figure 6. Schematic diagram of grain boundary hindering dislocations: (a) initial stage; (b) plastic deformation stage.

In addition, the deformation of FG steel can spread to more grains, so the stress distribution is more uniform than that of CG steel. Therefore, it is difficult for micropores and cracks to initiate and propagate, which ultimately increases the strength of the material.

Through microscopic observation, a large number of nano-scale cementite particles are found to be uniformly dispersed on the FG D6A steel matrix, as shown in Figure 2. The strength of the material is effectively improved by introducing nano-scale precipitates, which have been widely used in metal materials. Essentially, precipitation strengthening is achieved by generating small, high-hardness second-phase particles that hinder dislocation motion. At the same time, the interaction between cementite and dislocations is also enhanced, thereby strengthening the metal without greatly affecting the stiffness of the material [13]. Dislocations cannot shear hard cementite particles. In this case, dislocations will bypass particles through Orowan ring or cross-slip [14]. The strength increment is closely related to the volume fractions and size of the precipitated phase.

Figure 7 shows that the extrusion deformation between grains provides more nucleation sites for cementite, and the local temperature rise generated by plastic deformation also accelerates the nucleation process. Fresh dislocations appear around the cementite, and the dislocation density increases uninterruptedly. With the accumulation of plastic deformation, the degree of dislocation pile-up deepens. External force causes the cementite particles to move gradually and gather at the grain boundary. Moreover, cementite has a pinning effect on the grain boundaries, which makes it difficult for the grain boundary slip between grains to proceed and aggravates the stress concentration. Therefore, the interaction of dislocations, cementite and high-density grain boundaries results in FG D6A steel with ultra-high strength.

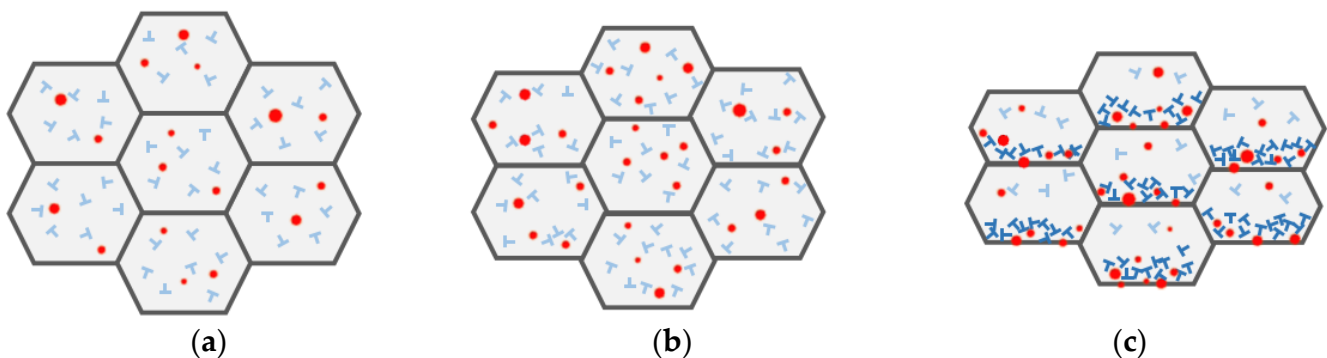


Figure 7. Schematic diagram of grain boundary and cementite hindering dislocations: (a) initial stage; (b) middle stage; (c) final stage.

Figure 8 presents the strength changes of CG/FG steel under static and dynamic tensile loading. D6A steel exhibits remarkable strain rate effect. As the strain rate changes from quasi-static to dynamic, the material strength increases significantly.

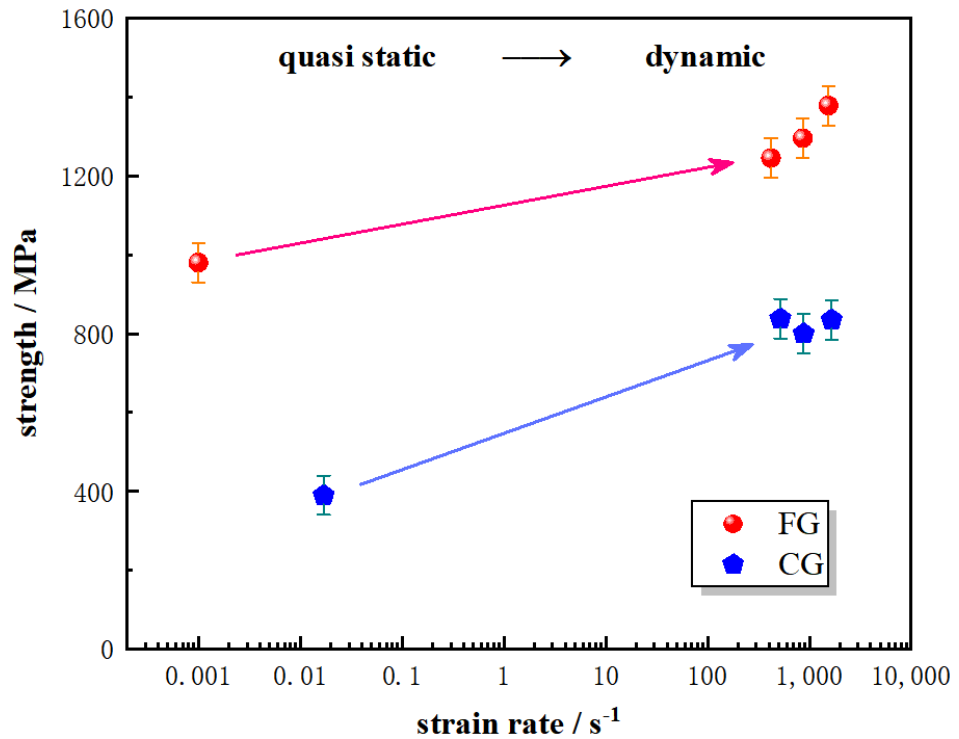


Figure 8. Quasi-static and dynamic tensile strength of D6A steel.

The fracture of the sample was observed by SEM to analyze the microstructure evolution of the investigated steel in the high-speed tensile test. Figure 9 shows the SEM image of the FG D6A steel after dynamic tensile deformation. The comparison shows that the microstructures under different strain rates are basically the same and mainly ferrite and cementite. However, with the increase in strain rate, the deformation of ferrite structure becomes increasingly intense, resulting in the increase in the total number of grains and grain boundary density, which enhances the hindrance of dislocation movement, and thus improves the dynamic strength of FG D6A steel.

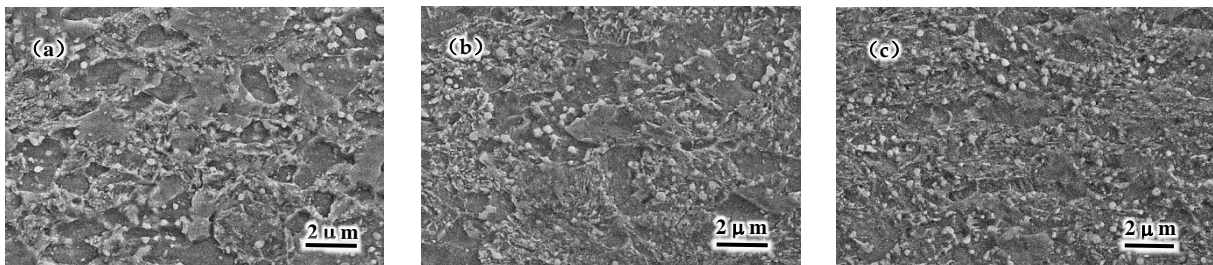


Figure 9. SEM micrograph of D6A steel after deformation: (a) 420 s⁻¹; (b) 860 s⁻¹; (c) 1540 s⁻¹.

Two parameters are generally used to describe the strain rate sensitivity of materials [15], namely the strain rate sensitivity coefficient m and the flow stress increment $\Delta\sigma$. Here, the strain rate sensitivity coefficient can be calculated as follows [16]:

$$m = \left(\frac{\partial \ln \sigma}{\partial \ln \dot{\epsilon}} \right)_T \approx \frac{\ln(\sigma_2 - \sigma_1)}{\ln(\dot{\epsilon}_2 - \dot{\epsilon}_1)} \quad (1)$$

where $\dot{\epsilon}$ is the strain rate and σ can be taken as the yield strength corresponding to different strain rates. In addition, the flow stress increment $\Delta\sigma$ can be expressed as follows:

$$\Delta\sigma = \sigma_d - \sigma_s \quad (2)$$

where, σ_d and σ_s are dynamic and static yield strength, respectively.

As shown in Table 3, the steel exhibits obvious strain rate effect in this experiment. The strain rate sensitivity coefficient m of the original CG steel was about 0.822~0.976 at room temperature, and the flow stress increment $\Delta\sigma$ was about 434 MPa. Compared with the quasi-static yield strength, the dynamic strength more than doubled, and the stress increment ratio reached 113.3%. The strain rate sensitivity coefficient m and flow stress increment $\Delta\sigma$ of FG steel are 0.816~0.923 and 326 MPa, respectively. Although the strength increment of FG steel under dynamic loading is slightly lower than that of the original CG steel, the strength increase ratio is very small, only about 33.2%. Therefore, as the average grain size decreases from 20 μm to 1.5 μm , the strain rate sensitivity of D6A steel shows a weakening trend.

Table 3. Strain rate sensitivity index of D6A steel (0.001~1500 s^{-1}).

Steel	m	$\Delta\sigma/\text{MPa}$	Stress Increment Ratio/%
CG	0.822~0.976	434	111.3
FG	0.816~0.923	326	33.2

The flow stress of UFG steel can be mainly divided into two parts [17]: thermal stress and non-thermal stress. Thermal stress corresponds to the thermal activation movement, which mainly overcomes the short-range barrier dependent on temperature and strain rate. Non-thermal stress is related to the long-range obstacles that cannot be overcome in the thermal activation process. The latter is almost independent of strain rate and temperature but largely affected by grain size. Jia established the following mechanical response function [18] in the study of UFG iron with BCC structure:

$$\tau = \tau_0 + \beta d^{-1/2} + g(\gamma) + \bar{\tau}_0 \left[1 - \left\{ \frac{kT}{\Delta G_{k0}} \ln \left(\frac{\dot{\gamma}_{k0}}{\dot{\gamma}} \right) \right\}^{\frac{2}{3}} \right] \quad (3)$$

The first three parts of the formula are the non-thermal stress dominated by initial lattice resistance and grain boundary strengthening effect, where $g(\gamma)$ is the strain hardening coefficient. The last part named Peierls-Nabarro stress is related to the short-range barrier, and it can be qualitatively judged that this stress component is related to the strain rate but has no direct relationship with the grain size, that is, the strain rate-dependent stress components have not changed greatly for different grain size steels. By contrast, when the size of D6A steel decreases from 20 μm to 1.5 μm , the grain boundary area increases greatly, and the non-thermal stress will occupy the main part of the flow stress. Therefore, in the same strain rate range, the proportion of strain rate-related thermal stress reduces gradually with the grain size refinement, and macroscopically, the strain rate sensitivity of FG D6A steel is weaker than that of original CG steel.

Furthermore, compared with CG steel, the strain hardening ability of FG D6A decreases under dynamic loading, and plastic instability begins to occur after the stress reaches the peak. This phenomenon deserves further study. Nevertheless, the stress softening phenomenon of some UFG materials [15] did not appear in the D6A steel.

4. Johnson–Cook Constitutive Model and Parameter Fitting

Establishing the constitutive model that can describe the plastic deformation behavior of materials is the premise of accurately simulating severe deformation processes such as impact [19]. In order to promote the application of FG D6A steel in aviation and military

fields, it is very important to find a constitutive model that can accurately describe its dynamic deformation behavior. The J–C model has become the most widely used phenomenological viscoplastic model for metallic materials due to its simple form and easy promotion of engineering application. The J–C model well describes the relationship between flow stress and plastic strain, strain rate and temperature. Its classical mathematical expression is as follows [20]:

$$\sigma = (A + B\varepsilon_p^n) \left(1 + C \ln \dot{\varepsilon}^*\right) (1 - T^{*m}) \quad (4)$$

Therein, σ reflects flow stress; A , B and n are strain-related material parameters at reference strain rates, where A is the yield strength. C is the coefficient describing the strain rate strengthening effect, and m is the factor describing the thermal softening effect. Here, ε_p is the equivalent plastic strain, and $\dot{\varepsilon}^*$ is the dimensionless equivalent plastic strain rate. T^* represents dimensionless temperature. as the temperature rise caused by dynamic loading is small, the thermal softening effect is not considered, so the value of m could be equal to 0. Finally, the simplified J–C model equation is obtained as follows:

$$\sigma = (A + B\varepsilon_p^n) \left(1 + C \ln \dot{\varepsilon}^*\right) \quad (5)$$

The material mechanical properties under different processes are often quite different, so it is necessary to determine the parameters combined with mechanical experiments. When loading at the reference strain rate, the J–C model is further simplified to the Ludwik–Hollomon formula [21]:

$$\sigma = (A + B\varepsilon_p^n) \quad (6)$$

According to the quasi-static loading stress–strain curve (Figure 5a), the yield strength of FG D6A steel is approximately about 980 MPa, that is, $A = 980$. Logarithmic transformation of the above formula can be obtained:

$$\ln(\sigma - A) = \ln B + n \ln \varepsilon_p \quad (7)$$

Fit the curve of $\ln(\sigma - A) - \ln \varepsilon_p$. As shown in Figure 10a, its slope is n , and B is obtained according to the intercept. Finally, the strain-related parameters can be calculated as follows: $B = 493$, $n = 0.625$. After the aforementioned parameters are determined, select the yield strength under different strain rates, and fit the curve. As shown in Figure 10b, the slope is the strain rate hardening coefficient, and $C = 0.026$.

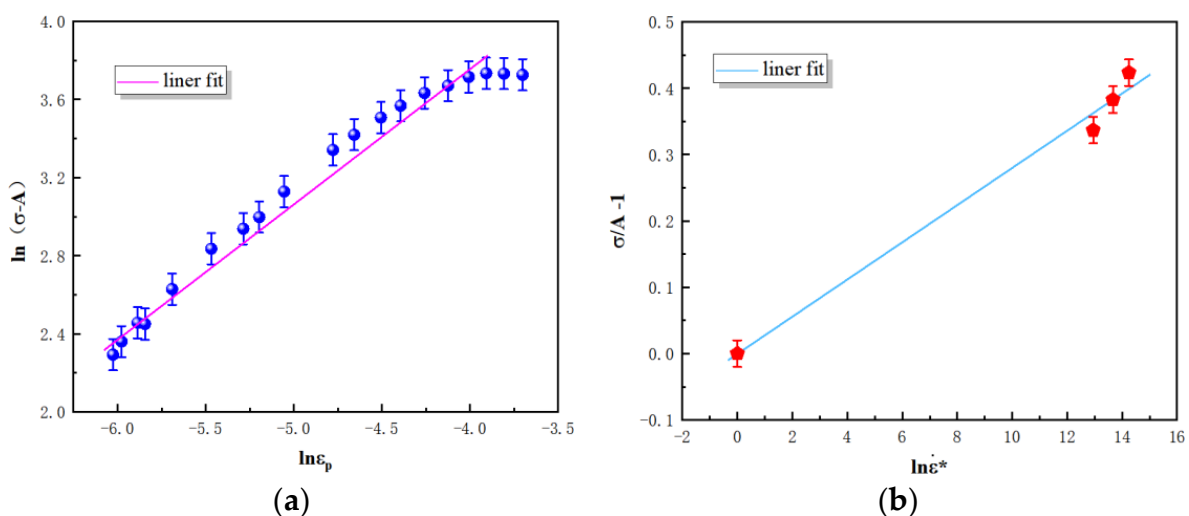


Figure 10. J–C constitutive model constants fitting results: (a) $\ln(\sigma - A) - \ln \varepsilon_p$; (b) $(\sigma/A - 1) - \ln \dot{\varepsilon}^*$.

In conclusion, the J–C model suitable for FG D6A steel at room temperature can be obtained from the data, as follows:

$$\sigma = \left(980 + 493\varepsilon_p^{0.625}\right) \left(1 + 0.026 \ln \dot{\varepsilon}^*\right) \quad (8)$$

A 3D specimen model is established, the size of which is consistent with the experimental specimen. The left end surface of the specimen is completely fixed, and the right end surface is given velocity boundary conditions to simulate loading at different strain rates. Hexahedral elements were selected for the mesh, and the mesh in the middle was appropriately refined. Select the J–C model that was built in the software and input the above-mentioned relevant parameters. Of note, the elastic modulus of FG D6A steel is 210 GPa. Loading simulations at different strain rates were carried out in ABAQUS software using explicit dynamic analysis type.

Figure 11a shows the nephogram of finite element tensile simulation results. As can be observed, the specimen generates stress concentration in the middle. Calculate the mechanical information of the middle part, plot the stress–strain curve and synchronously compare with the experimental data, as shown in Figure 11b. The results indicate that the stress value of the simulation results is basically consistent with the experimental data. Several stress values under the same strain are selected from the experimental data and the numerical simulation curve, and the comparison shows that the average error in the hardening stage maintains within 15%. Therefore, the parameters accurately describe the dynamic mechanical behavior of FG D6A steel at a certain range of strain rate in our tests.

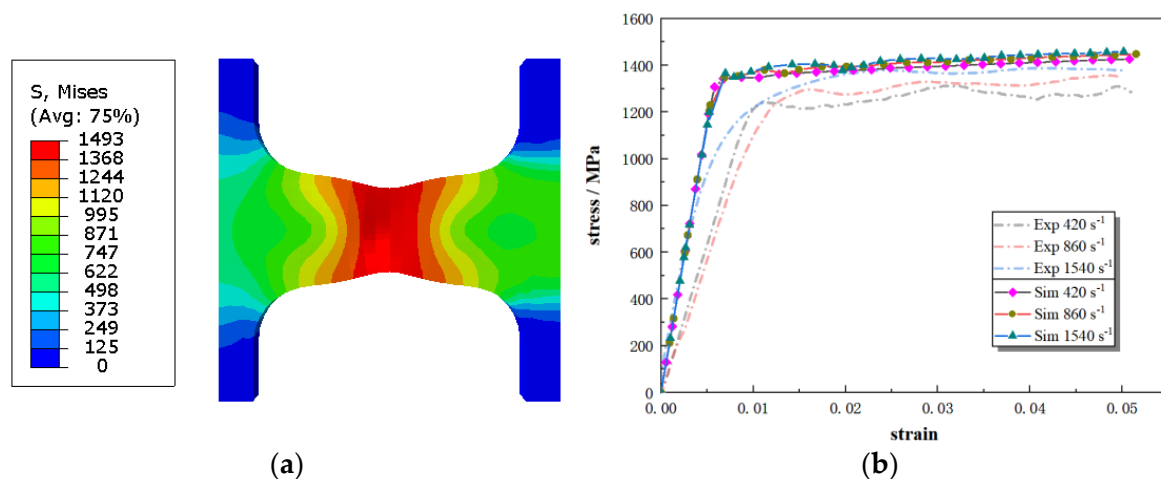


Figure 11. Finite element calculation results of tensile loading of FG D6A steel by using the J–C model: (a) stress cloud; (b) comparison of the result with experimental data.

5. Conclusions

In this study, the quasi-static and dynamic mechanical properties of D6A steel were investigated by using a material testing machine and rotating disk Hopkinson tension bar. From the microscopic point of view, the influence of grain refinement on the macroscopic mechanical properties of materials such as strength and work hardening ability was discussed, and the reasons for the decrease in strain rate sensitivity with the decrease in grain size was analyzed simultaneously. The parameters of the classical J–C model were fitted based on the experimental results. The relevant results can provide certain reference value for promoting the practical application of FG D6A steel, as follows:

1. Grain refinement and cementite precipitation are the main reasons for the strength improvement of FG D6A steel. High-density grain boundaries and hard precipitates improve the strength of the material by hindering dislocation movement. In addition, the investigated steel shows obvious strain rate effect, which is considered to be

the result of grain crushing that further enhances the fine-grain strengthening effect during dynamic loading.

2. Grain refinement reduces the strain rate sensitivity of the investigated steel. According to the existing mechanical response model, the reason is that the non-thermal stress related to grain size in the FG steel increases significantly and occupies the dominant part of the total flow stress.
3. The J–C model suitable for FG D6A steel at room temperature was obtained as follows: $\sigma = (980 + 493\varepsilon_p^{0.625}) (1 + 0.026 \ln \dot{\varepsilon}^*)$. Combined with the finite element calculation result, this model can effectively predict the dynamic mechanical behavior of FG D6A steel.

Author Contributions: Conceptualization, X.F.; methodology, X.F., X.Z., Z.Y. and Y.S.; software, Z.Y.; investigation, X.F., X.Z., Y.S., R.X. and X.H.; writing—original draft preparation, Z.Y.; writing—review and editing, X.F. and Y.S. All authors have read and agreed to the published version of the manuscript.

Funding: This research was funded by the National Natural Science Foundation of China, grant number 12102413.

Institutional Review Board Statement: Not applicable.

Informed Consent Statement: Not applicable.

Data Availability Statement: Not applicable.

Acknowledgments: The authors gratefully acknowledge the financial support from the National Natural Science Foundation of China with Grant No. 12102413. The authors also gratefully acknowledge the experimental support from the Chinese Academy of Engineering Physics and Northeastern University.

Conflicts of Interest: The authors declare no conflict of interest.

References

1. Calcagnotto, M.; Adachi, Y.; Ponge, D.; Raabe, D. Deformation and fracture mechanisms in fine- and ultrafine-grained ferrite/martensite dual-phase steels and the effect of aging. *Acta Mater.* **2011**, *59*, 658–670. [[CrossRef](#)]
2. Pang, Q.H.; Li, W.J.; Cai, M.Y.; Qi, H.; Zhang, C.C.; Wu, J.N. The investigation of strength and plasticity mechanism of low-temperature annealed ultrafine grained stainless steel. *IOP Conf. Ser. Mater. Sci. Eng.* **2018**, *372*, 1–9. [[CrossRef](#)]
3. Park, K.T.; Shin, D.H. Microstructural interpretation of negligible strain-hardening behavior of submicrometer-grained low-carbon steel during tensile deformation. *Metall. Mater. Trans. A* **2002**, *33*, 705–707. [[CrossRef](#)]
4. Liu, J.J.; Suo, T.; Fan, Y.Q.; Li, J.G.; Zhou, F.H.; Li, Y.L. Dynamic mechanical responses of ultrafine-grained IF steel over a wide range of temperatures. *Int. J. Appl. Mech.* **2018**, *10*, 1–20. [[CrossRef](#)]
5. Khan, A.; Chen, X. Nanocrystalline aluminum and iron: Mechanical behavior at quasi-static and high strain rates, and constitutive modeling. *Int. J. Plast.* **2004**, *22*, 195–209. [[CrossRef](#)]
6. Zheng, Z.G.; Xie, C.J.; Sun, T.; Yuan, S. A mixed hardening model of ultrafine-grained materials and numerical simulation. *J. Mech. Eng.* **2014**, *50*, 77–83. [[CrossRef](#)]
7. Wang, C.X.; Shi, L.; Xu, J.; Shan, D.; Guo, B. Constitutive relationship of micro-deformation in an ultrafine-grained pure aluminum. *Mater. Sci. Technol.* **2016**, *24*, 1–7. [[CrossRef](#)]
8. Wang, P.J.; Shen, Y.F.; Feng, X.W.; Wang, H.B.; Yang, S.Q. Microstructures and textures of ultrafine grained D6A steel by using rolling and annealing. *J. Iron Steel Res.* **2016**, *28*, 54–59. [[CrossRef](#)]
9. Jia, N.; Shen, Y.F.; Liang, J.W.; Feng, X.W.; Wang, H.B.; Misra, R.D.K. Nanoscale spheroidized cementite induced ultrahigh strength-ductility combination in innovatively processed ultrafine-grained low alloy medium-carbon steel. *Sci. Rep.* **2017**, *7*, 2679. [[CrossRef](#)] [[PubMed](#)]
10. Liang, J.W.; Shen, Y.F.; Zhang, C.S.; Feng, X.W.; Wang, H.B.; Sun, X. In situ neutron diffraction in quantifying deformation behaviors of nano-sized carbide strengthened UFG ferritic steel. *Mater. Sci. Eng. A* **2018**, *726*, 298–308. [[CrossRef](#)]
11. Liang, J.W.; Shen, Y.F.; Misra, R.D.K.; Liaw, P.K. High strength-superplasticity combination of ultrafine-grained ferritic steel: The significant role of nanoscale carbides. *J. Mater. Sci. Technol.* **2021**, *83*, 131–144. [[CrossRef](#)]
12. Zhang, X.L.; Feng, X.W.; Shen, Y.F. Toughening mechanism of D6A steel during rolling process. *J. Mater. Eng.* **2021**, *50*, 1–15. [[CrossRef](#)]
13. Zhang, Z.F.; Lu, L. *Mechanical Behaviour of Materials*; Higher Education Press: Beijing, China, 2017; pp. 596–603.
14. Gladman, T. Precipitation hardening in metals. *Mater. Sci. Technol.* **1999**, *15*, 30–36. [[CrossRef](#)]

15. Okitsu, Y.; Takata, N.; Tsuji, N. Dynamic deformation behavior of ultrafine-grained iron produced by ultrahigh strain deformation and annealing. *Scr. Mater.* **2011**, *64*, 896–899. [[CrossRef](#)]
16. Liu, X.Y.; Zhang, Q.; Yang, X.R. Deformation, strain rate sensitivity and activation volume of ultrafine-grained commercially pure Ti. *Rare Met. Mater. Eng.* **2020**, *49*, 1867–1872.
17. Meyers, M.A. *Dynamic Behavior of Materials*; John Wiley & Sons: New York, NY, USA, 1994; p. 340.
18. Jia, D.; Ramesh, K.T.; Ma, E. Effects of nanocrystalline and ultrafine grain sizes on constitutive behavior and shear bands in iron. *Acta Mater.* **2003**, *51*, 3495–3509. [[CrossRef](#)]
19. Hu, X.; Xie, L.J.; Gao, F.N.; Xiang, J. On the development of material constitutive model for 45CrNiMoVA ultra-high-strength steel. *Metals* **2019**, *9*, 374. [[CrossRef](#)]
20. Johnson, G.R.; Cook, W.H. Fracture characteristics of three metals subjected to various strains, strain rates, temperatures and pressures. *Pergamon* **1985**, *21*, 31–48. [[CrossRef](#)]
21. Bergstrom, Y.; Aronsson, B. The application of a dislocation model to the strain and temperature dependence of the strain hardening exponent n in the Ludwik-Hollomon relation between stress and strain in mild steels. *Metall. Trans.* **1972**, *3*, 1951–1957. [[CrossRef](#)]